**The EMBO Journal (2013) 32,** 677–687
www.embojournal.org

OPEN ACCESS TRANSPARENT PROCESS

THE EMBO JOURNAL

# Structural insights into the regulation of cohesion establishment by Wpl1

**Avradip Chatterjee, Silva Zakian, Xiao-Wen Hu and Martin R Singleton***

Macromolecular Structure and Function Laboratory, Cancer Research UK, London Research Institute, London, UK

**Correct segregation of duplicated chromosomes to daughter cells during mitosis requires the action of the cohesin complex. This tripartite ring-shaped molecule is involved in holding replicated sister chromatids together from S phase until anaphase onset. Establishment of stable cohesion involves acetylation of the Smc3 component of cohesin during replication by the Eco1 acetyltransferase. This has been proposed to antagonise the activity of another member of the cohesin complex, Wpl1. Here, we describe the X-ray structure of the conserved Wapl domain, and demonstrate that it binds the ATPase head of the Smc3 protein. We present data that suggest that Wpl1 may be involved in regulating the ATPase activity of cohesin, and that this may be subject to the acetylation state of Smc3. In addition, we present a structure of the Wapl domain bound to a functionally relevant segment of the Smc3 ATPase.**
*The EMBO Journal* (2013) **32,** 677–687. doi:10.1038/emboj.2013.16; Published online 8 February 2013
*Subject Categories:* cell cycle; structural biology
*Keywords*: cohesin; cohesion; structural biology; Wpl1

## Introduction

Correct chromosome segregation in eukaryotes is ensured by physically linking duplicated sister chromatids during the S phase of the cell cycle and maintaining this connection until anaphase onset (Nasmyth, 2001). The linkage between sister chromatids is maintained by the ring-shaped cohesin complex (Haering *et al*, 2008), which is loaded onto chromosomes in late G1 phase and activated in a multi-step, replication-dependent manner (Skibbens *et al*, 1999; Tóth *et al*, 1999; Skibbens, 2009). The core of the cohesin complex consists of three proteins, Smc1, Smc3, and Scc1. Smc1 and Smc3 are members of the Structural Maintenance of Chromosomes family and contain a globular ABC ATPase domain connected to a dimer-forming hinge domain by long intramolecular coiled coils, which are proposed to entrap sister DNA strands (Hirano, 2002). Scc1 is a member of the kleisin family of proteins that bridges the ATPase heads of the Smc1–Smc3 ring (Schleiffer *et al*, 2003). Proteolytic cleavage of this subunit by separase at anaphase onset allows release and poleward movement of the chromosomes (Uhlmann *et al*, 2000). In budding yeast, all chromosome-bound cohesin is removed at this point. In vertebrates, by contrast, the bulk of cohesin is removed from chromosomes during prophase in a proteolysis-independent manner (Losada *et al*, 1998; Waizenegger *et al*, 2000; Sumara *et al*, 2002), while centromeric cohesin is protected until anaphase by the protein Sgo1, at which point it is proteolytically released (Kitajima *et al*, 2004; Salic *et al*, 2004; Tang *et al*, 2004; McGuinness *et al*, 2005).

Prior to DNA replication, cohesin binds chromatin in a reversible manner that is not capable of maintaining cohesion and is thought to be held in this state by a complex containing the proteins Wpl1 and Pds5 (Tanaka *et al*, 2001; Gandhi *et al*, 2006; Kueng *et al*, 2006; Ben-Shahar *et al*, 2008; Rowland *et al*, 2009; Sutani *et al*, 2009), whose activity is antagonised by Eco1-mediated acetylation of the Smc3 protein during S phase (Ivanov *et al*, 2002; Bellows *et al*, 2003; Lengronne *et al*, 2006; Ben-Shahar *et al*, 2008; Unal *et al*, 2008; Zhang *et al*, 2008). In vertebrates, the stably chromatin-bound form of cohesin may be maintained by the binding of the protein sororin to Pds5 (Schmitz *et al*, 2007; Nishiyama *et al*, 2010) though it is unclear if this system is conserved in yeast.

The *Wapl* gene was initially identified in *Drosophila* as a controller of heterochromatin structure and cohesion (Vernì *et al*, 2000). Subsequent studies in vertebrates have shown that the protein is involved in the non-proteolytic removal of cohesin during the prophase pathway as well as interphase (Gandhi *et al*, 2006; Kueng *et al*, 2006). Wapl shows homology to the budding yeast Rad61 protein (Game *et al*, 2003; Warren *et al*, 2004) which, when mutated, allows bypass of lethality associated with Eco1 inactivation (Ben-Shahar *et al*, 2008; Unal *et al*, 2008). Collectively, these results suggest that Wapl is involved in the destabilisation of chromatin-bound cohesin in an acetylation-dependent manner, and that budding yeast Rad61 (now also known as Wpl1) mediates a similar process. Currently, the molecular mechanisms of this complex pathway are not fully understood. In this paper, we present results of structural and biochemical studies of the Wpl1 protein. We describe the structure of the conserved domain of the Wpl1 protein, and present a biochemical analysis of its interactions with other members of the cohesin complex, which provides new insights into the process of cohesin establishment.

## Results

### *Structure of the Wapl domain*

All Wapl orthologues contain a C-terminal conserved domain (Figure 1A; Supplementary Figure 1a), which defines the family. This domain is ~45 kDa in size, and was predicted to be predominantly α-helical (Kueng *et al*, 2006). The non-conserved N-terminal of the protein is highly divergent in both length and composition, and is responsible for mediating interactions with Pds5 (Shintomi and Hirano, 2009). Secondary structure predictions of the protein

*Corresponding author. Macromolecular Structure and Function Laboratory, Cancer Research UK, London Research Institute, 44 Lincoln's Inn Fields, London WC2A 3LY, UK. Tel.: +44 (0) 207 269 3148; Fax: +44 (0) 207 269 3258; E-mail: martin.singleton@cancer.org.uk

**Received: 29 August 2012; accepted: 10 January 2013; published online: 8 February 2013**

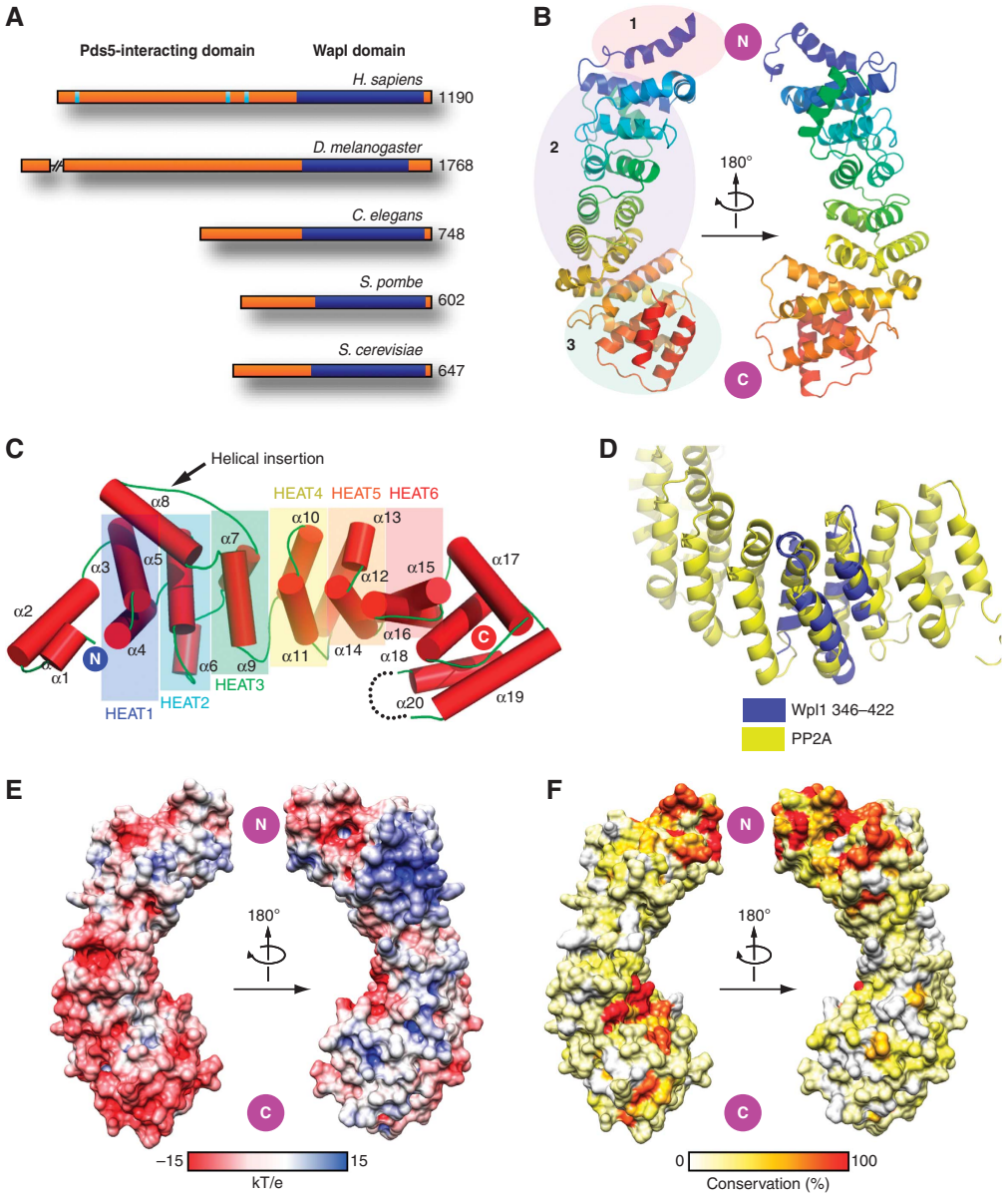


**Figure 1** Structure of the Wapl domain. (**A**) Domain structure of four Wapl orthologues showing the location of the conserved Wapl domain (blue). The length of the protein is indicated. Pale blue bars indicate the location of the Pds5-interacting FGF repeats in the human protein. (**B**) Ribbon diagram of AgWpl1$^{184–561}$, coloured blue (N-terminal) to red (C-terminal). The protein is subdivided into three indicated domains with the HEAT repeats comprising domain 2. (**C**) Secondary structural elements of the *A. gossypii* Wapl domain. Helices are numbered, and position of the canonical HEAT repeats highlighted. The position of the helical insertion in repeat HEAT3 is indicated. (**D**) Structure-based superimposition of the central Wpl1 HEAT repeats onto the PP2A repeats (pdb i.d. 1b3u). Wpl1 is shown in blue and PP2A in yellow. (**E**) Electrostatic surface of the Wapl domain showing positive potential in blue and negative in red. (**F**) Surface conservation properties of the Wapl domain. Red indicates areas of high conservation, white of low.

suggest that this divergent N-terminal is likely to be intrinsically disordered, so we decided to further investigate the structure of the conserved C-terminal Wapl domain. We identified a truncation of the Wpl1 protein from *Ashbya gossypii* (transcript AAR187C) comprising the Wapl domain that yielded high-quality crystals. The *A. gossypii* Wpl1 (AgWpl1) protein is fractionally shorter than budding yeast equivalent, but shows a high degree of similarity and 24% identity over the entire sequence (Supplementary Figure 1b). The final construct crystallised contained residues 184–561 of AgWpl1, corresponding to residues 271–635 of budding yeast Wpl1 (ScWpl1). High quality diffraction data were obtained to a resolution of 2.1 Å, and the structure was determined using multiple wavelength anomalous diffraction of a selenomethionine-substituted derivative. Statistics relating to the X-ray analysis are presented in Supplementary Table 1. The majority of the peptide chain is clearly defined in the electron density, with only short breaks between residues 544–548 (chain A) and 189–194, 214–221, 311–312 (chain B). The overall model refinement statistics are appropriate to the resolution of the experimental data.

The Wapl domain forms an elongated, peanut-shaped structure of ~90 × 35 Å (Figure 1B). The fold is defined by 20 consecutive α-helices and may be divided into 3 subdomains (Figure 1C). Domain 1 (residues 189–220) forms an anti-parallel helical 'cap' to the structure, and is followed by

 

six HEAT repeats that form the central domain of the protein. The C-terminal lobe (domain 3, residues 420–561) is composed of a flattened 4-helix bundle capped by two antiparallel helices at the extreme C-terminal. Three-dimensional homology searches performed using the DALI server (Holm and Sander, 1993) readily identify the central HEAT core of the protein and the Wapl repeats may be aligned to those of human PP2A (Groves *et al*, 1999) with a Cα r.m.s. deviation of 3.9 Å over 72 residues (Figure 1D). No obvious structural homologues to domains 1 and 3 were identified. The topology of the helices in these domains is the same as in the HEAT repeat, but the three-dimensional structure has substantially diverged from the basic repeat architecture. An unusual feature of the structure is an insertion of a long helix and connecting loop (residues 301–329) into repeat HEAT3 that projects away from the main body of the protein, somewhat like an opposable thumb against a palm formed by domain 1 (Figure 1C). Analysis of the electrostatic surface of the protein (Figure 1E) showed that the N-terminal domain is highly charged with prominent acidic and basic patches, while the C-terminal domain is generally acidic or uncharged. Mapping sequence conservation onto the molecular surface identifies regions of particular interest, two corresponding to the charged patches in the N-lobe of the protein, and a conserved hydrophobic patch on the inner face of the C-terminal lobe (Figure 1F). Based on our structural analyses and multiple sequence alignments of the Wapl domain, we have defined five sequence motifs that constitute these three surface features (Figure 2). Motifs 1 and 2 form the N-terminal acidic and basic regions, while motifs 3, 4, and 5 form the C-terminal hydrophobic patch.

### *Screening for interactions between the Wapl domain and the cohesin complex*

It has previously been shown that Wapl directly interacts with Pds5 in both yeast and vertebrates via the N-terminal domain (Gandhi *et al*, 2006; Kueng *et al*, 2006; Shintomi and Hirano, 2009; Sutani *et al*, 2009), but the function of the conserved C-terminal domain was unknown. We therefore decided to analyse the interactions between this domain and other proteins in the cohesin complex in more detail. To identify putative interacting partners, we performed a screen against a membrane peptide array comprising the AgSmc1 and AgSmc3 ATPase heads and AgScc1. The arrays consisted of

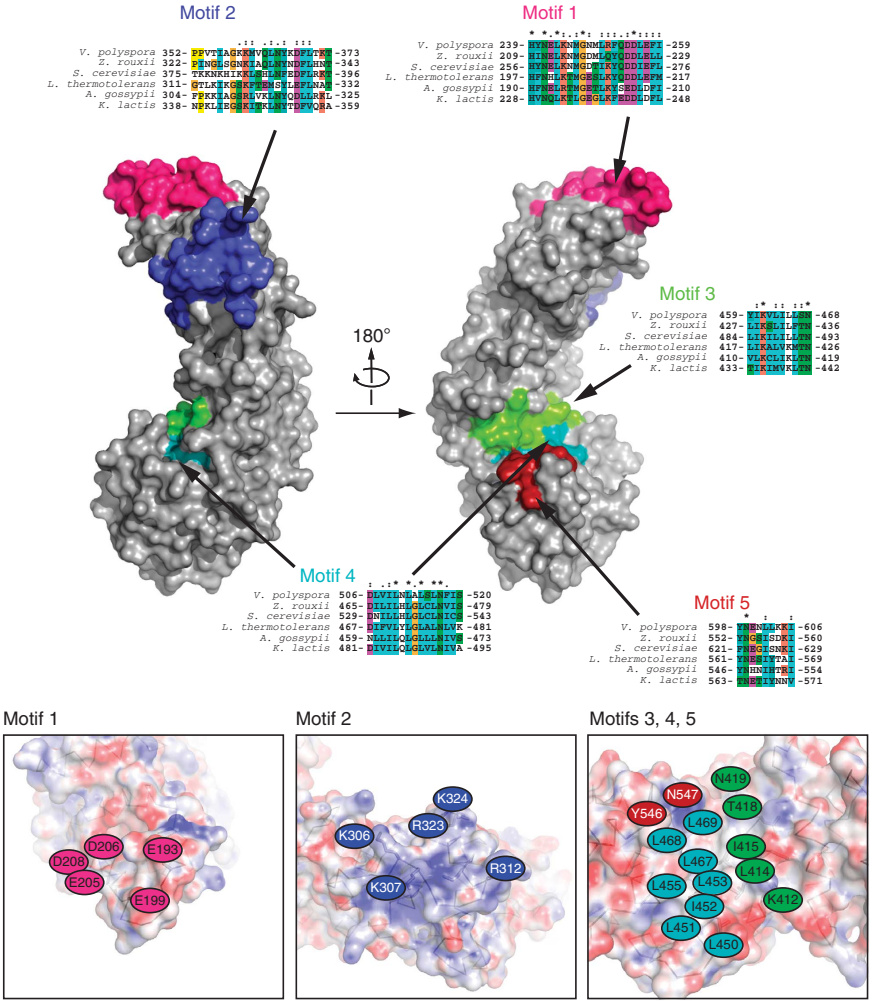


**Figure 2** Conserved motifs in the Wapl domain. The positions of the five sequence- and structure-based motifs are mapped onto the surface representation of the protein, and multiple sequence alignments of the corresponding residues in six fungal Wpl1 orthologues indicated. The residues in the *A. gossypii* sequence are indicated against electrostatic representations of the protein surface. Motif 2 is relatively weakly conserved at a sequence level, but characterised by a basic-residue rich tract that falls in the α8 helical insertion and connecting loop. The sequences shown are from *V. polyspora*, *Z. rouxii*, *S. cerevisiae*, *L. thermotolerans*, *A. gossypii*, and *K. lactis*.

21-mer peptides covering the proteins at a 3-residue resolution. These were probed with the isolated Wapl domain. We obtained strong hits against three sequences in AgSmc3, labelled WIS1, WIS2, and WIS3 (*W*apl *I*nteracting *S*equence; Figures 3A and B and Supplementary Figure 2a), as well as some potential hits, primarily on the N-terminal of AgScc1 (Supplementary Figure 2b). Interestingly, it is the N-terminal of Scc1 that interacts with Smc3, raising the possibility that the Wapl domain may interact with both proteins simultaneously, independently of Pds5 (Shintomi and Hirano, 2009). However, these potential Scc1 interactions have not been further tested in the current study. The AgSmc3 target peptides identified all mapped to regions predicted to be solvent exposed based on analysis of the homologous ScSmc1 crystal structure (Haering *et al*, 2004; Figure 3C) and are all highly conserved between Smc3 orthologues. WIS1 lies across two strands and the interconnecting loop at the top of the external β-sheet of the ATPase domain. Intriguingly, the connecting loop in the centre of the sequence also contains lysines K107 and K108 that correspond to the Eco1-targetted lysines K112 and K113 in ScSmc3. WIS2 constitutes two short α-helices and connecting loops that lie over the ATP-binding sites. These connect the so-called Q-loop that interacts with the bound nucleotide to the base of the coiled-coil domain. The WIS3 site is located at the base of the outer helix that forms the coiled-coil domain and extends through a short loop (disordered in the crystal structure) to the adjacent β-strand. There is some uncertainty in mapping the exact location of this site to the Smc1 structure, as the sequence of this region differs significantly between Smc3 and Smc1.

### *Binding site validation and analysis*

To validate the hits obtained in the peptide array, and obtain quantitative data on the binding, we analysed the interactions between the peptides and the Wapl domain by fluorescence polarisation (FP) assays. We used peptides corresponding to the *A. gossypii* sequences carrying an amino-terminal fluorescein group and purified recombinant Wapl domain. The binding curves and derived constants are shown in Figure 4. All three peptides bound with high micromolar affinities. We next analysed a variant of the WIS1 in which lysines K107 and K108 were replaced by ε-acetyl lysine, representing the acetylated state. Interestingly, this modification substantially reduced, but did not eliminate binding of the peptide to the Wapl domain. We next decided to verify these results and the affect of lysine acetylation in the context of the intact proteins by analysing the binding of the Wapl domain to an intact Smc3 globular head. We made a construct containing the full *Saccharomyces cerevisiae* Smc3 ATPase domain with the coiled coils and hinge replaced by a short flexible linker (Supplementary Figures 2c and d) to create a monopartite ATPase head (ScSmc3$^{AH}$). One complication that arose was the finding that the Smc3 heads cannot be acetylated *in vitro* with Eco1 (Borges *et al*, 2010). We therefore made a mutant version of the protein, where lysines 112 and 113 were replaced with asparagines as this has previously been shown to recapitulate the effect of acetylation (Ben-Shahar *et al*, 2008; Unal *et al*, 2008). The affinities were quantified using a surface-based bio-layer interferometry system (ForteBio Octet) with the ScWpl1$^{259–647}$ being coupled to the surface and ScSmc3$^{AH}$ in solution. The data obtained allowed excellent fits for both association and dissociation

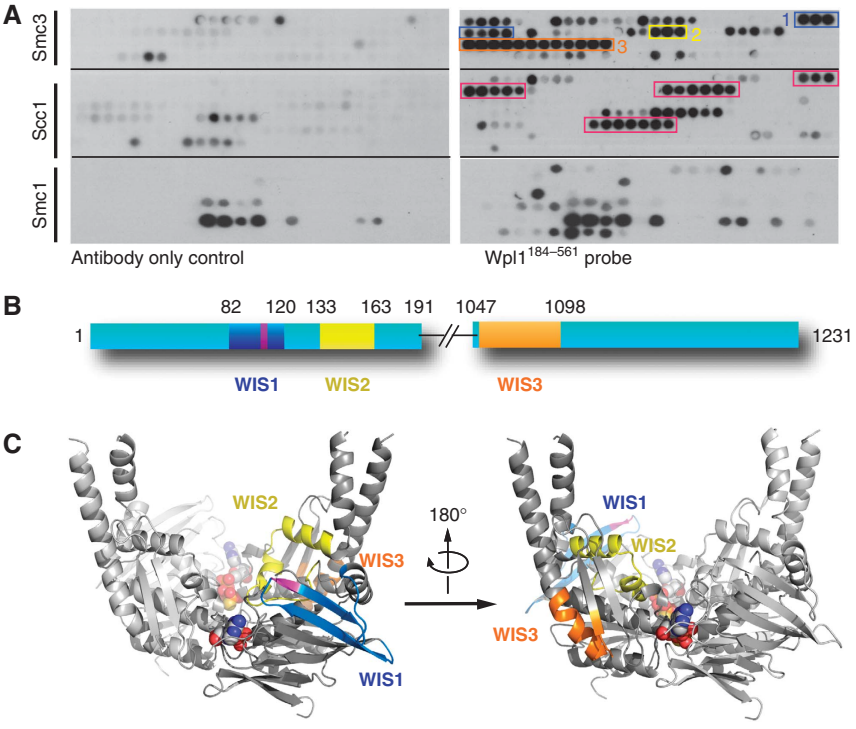


**Figure 3** Screening of potential Wapl domain interactors. (**A**) Peptide array screen of potential Wapl domain binding partners in the AgSmc3/AgSmc1 ATPase heads and AgScc1. The likely positive hits are boxed and numbered. (**B**) Schematic of Smc3 primary structure showing the position of the target peptides. The coiled-coil domain is omitted for clarity. (**C**) Structure of the ScSmc1 protein (pdb i.d. 1w1w) with the sequences homologous to WIS1–WIS3 indicated in the same colour scheme as in (**A**) and (**B**) mapped onto the ribbon diagram of one monomer.

curves with no non-specific binding observed to the sensor or GST tag (Supplementary Figure 2e). The binding parameters are shown in Table I. The full-length intact protein domains demonstrated considerably higher affinity compared to the experiments with the isolated peptides, presumably because of cooperative binding at multiple sites. As can be seen, $Smc3^{AH\ K112N,\ K113N}$ reproducibly shows a significantly lower affinity for the Wapl domain than the wild-type protein. Although the lysine to asparagine mutation bypasses the requirement for Eco1 *in vivo*, it probably does not represent a true acetyl lysine mimicking mutation *in vitro*. We would expect the difference in affinity to be greater against the natural acetylated substrate as the terminal methyl group of ε-acetyl lysine is chemically more distinct from the lysine ε-amine than the amide moiety in asparagine. Analysis of other lysine mutants (Rowland *et al*, 2009) suggests that neutralisation of the basic lysine side chain is the key function of acetylation, rather than formation of a specific side-chain interaction.

### *Structure of the Wapl domain bound to $Smc3^{154–163}$*

To gain structural insights into interaction between Wpl1 and cohesin, we attempted to determine the crystal structure of the Wapl domain bound to the Smc3 target peptides. We were successful in obtaining a structure of the protein bound to the WIS2 peptide at 2.01 Å resolution (Supplementary Table 1). Clear electron density was seen for residues 154–163 of Smc3 and allowed unambiguous assignment of the sequence (Figures 5A and B; and Supplementary Figure 3a). The peptide lies in the hydrophobic pocket on the surface of Wpl1 formed by motifs 3, 4, and 5. Residues 159–163 form a single α-helical turn, with the remainder of the peptide in an extended conformation. The primary interaction between the peptide and Wpl1 is formed between the conserved leucine residues L158 and L161 of Smc3 projecting into the hydrophobic cavity formed by helices α16, α17, α19, and α20 (Figure 5C; Supplementary Figure 3b). Acidic residues E162 and E163 form polar interactions primarily with main and side chains of N419, H548, and N549, as well as main chain carbonyl hydrogen bonds to the N547 side-chain amide. The N-terminal end of the peptide is more loosely bound to Wpl1 and curves away from the side of the binding cavity. Comparison to the equivalent helix in the Smc1 crystal structure (Figure 5D) shows that the C-terminal end of the peptide remains in a helical conformation. The terminal hydrophobic and acid pairs of residues that interact with Wpl1 are in an equivalent position to the chemically similar residues in Smc1. However, the N-terminal of the peptide is somewhat unwound and deviates from the Smc1 structure. It is not clear if this reflects the conformation that exists in unbound Smc3, though the N-terminal end of the peptide diverges considerably in amino-acid composition between Smc1 and Smc3, which might account for the differing secondary structure. This helix is disordered in certain structures of related ABC ATPases (Hopfner *et al*, 2000), and other studies have suggested it can adopt multiple conformations (see Discussion) indicating that the form bound to Wpl1 might relate to a specific intermediate in the catalytic cycle.

**Table I** $ScWpl1^{259–647}$-$ScSmc3^{AH}$ binding affinities

| Proteins | KDa (nM) | $K_{on}$ ($1/Ms \times 10^3$) | $K_{off}$ ($1/s \times 10^{-4}$) | $R^2$ |
|---|---|---|---|---|
| Wild-type Smc3/Wild-type Wpl1 | 47 | 5.22 ± 0.07 | 2.48 ± 0.08 | 0.996 |
| Smc3 K112N K113N | 88 | 4.88 ± 0.06 | 4.31 ± 0.11 | 0.993 |
| Smc3 L163A L166A D168A | 104 | 4.77 ± 0.06 | 4.97 ± 0.12 | 0.993 |
| Smc3 L163D L166D | 102 | 5.88 ± 0.08 | 5.97 ± 0.12 | 0.989 |
| Wpl1 N493A N622A L532E | 82 | 4.20 ± 0.03 | 3.44 ± 0.06 | 0.998 |
| Wpl1 N493A N622A L577R | 77 | 5.54 ± 0.06 | 4.28 ± 0.10 | 0.993 |
| Wpl1 N493E N622E | 126 | 3.92 ± 0.05 | 4.92 ± 0.09 | 0.995 |
| Wpl1 D271A D272A | 167 | 2.37 ± 0.03 | 3.95 ± 0.06 | 0.998 |
| Wpl1 K376Q K377Q K382Q K383Q | 200 | 2.80 ± 0.04 | 5.60 ± 0.07 | 0.997 |

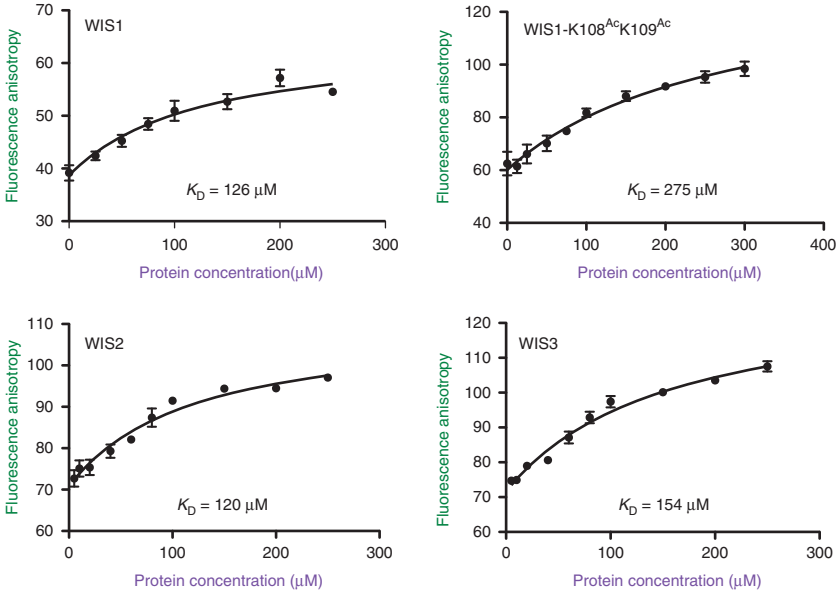


**Figure 4** Quantification of peptide binding. Fluorescence polarisation binding curves for the peptides WIS1–WIS3, and the K107Ac K108Ac derivative of WIS1, together with derived binding constants.

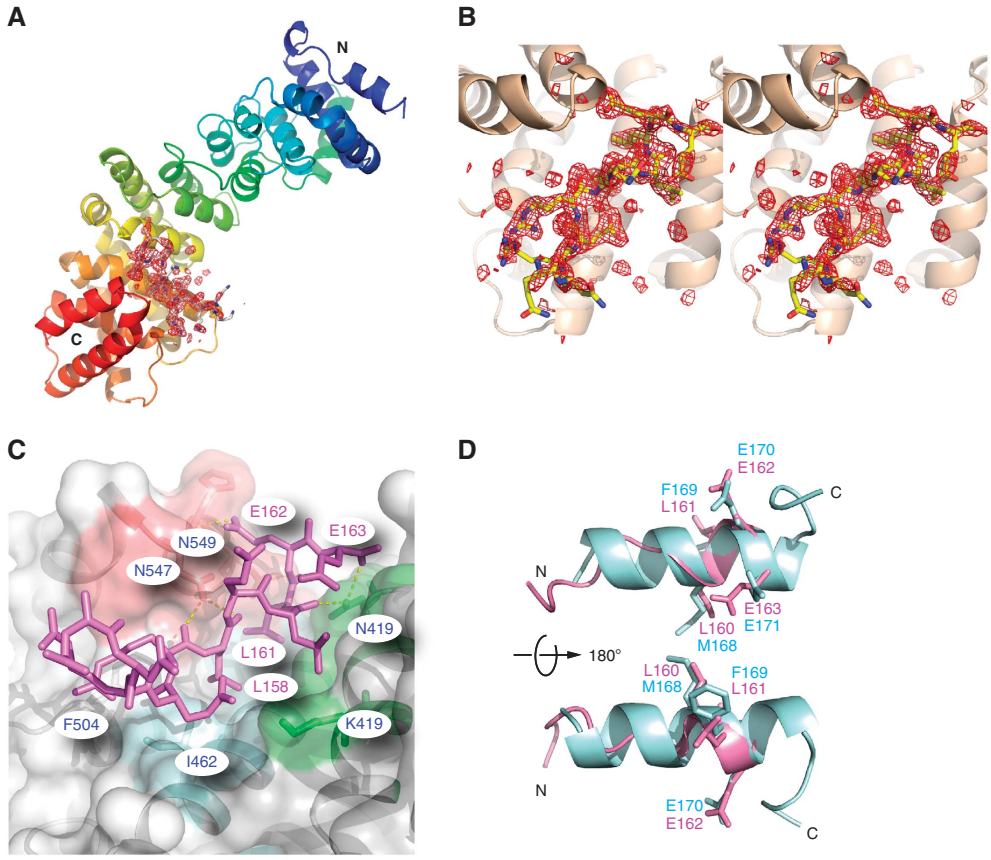


**Figure 5** Details of Wpl1–Smc3 interactions. (**A**) Ribbon diagram of the AgWpl1$^{184–561}$–WIS2 complex. The Wapl domain is shown as a ribbon, and electron density for the peptide in an unbiased |Fo| − |Fc| omit map contoured at 2σ is depicted in red. (**B**) Stereo close-up of the electron density for the WIS2 peptide calculated as in (**A**). The peptide is indicated in yellow. (**C**) Close-up of the peptide-binding site. The hydrophobic surface on the Wapl domain comprising motifs 3, 4, and 5 (green, blue, and red, respectively). The WIS2 peptide is shown in pink. Residues from Wpl1 (blue) or Smc3 (pink) that participate in interactions are labelled. (**D**) Comparison of the WIS2 peptide as bound to the Wapl domain (pink) and the equivalent sequence in the Smc1 crystal structure (cyan). The matching residues at the C-terminal of the helix that participate in interactions with Wpl1 are labelled.

### *Biochemical and in vivo characterisation of Wpl1–Smc3 interactions*

Our experiments have shown that mutations in the WIS1 peptide that mimic Smc3 acetylation reduce the affinity of Wpl1 for Smc3, and these mutations have previously been shown to be active *in vivo*, by allowing *eco1-1* bypass (Ben-Shahar *et al*, 2008; Unal *et al*, 2008; Rowland *et al*, 2009). To further study the function of other interactions involving WIS2, WIS3, and the conserved Wapl motifs (Figure 6A), we carried out binding studies using structure-guided mutants that we predict would affect the Wpl1–WIS2 interface, as well as on conserved residues in Wpl1 motifs 1 and 2. Correct folding of all the mutant proteins was verified by thermal denaturation assays and gel filtration (Supplementary Figure 4). Affinities were measured using purified recombinant ScWpl1$^{259–647}$ and ScSmc3$^{AH}$ as described previously. Mutations in the Wpl1–WIS2 interface were made in both proteins, and resulted in an approximate halving of affinity (Figure 6B; Table I), with similar effects being caused by mutations in either protein. The strongest effect was observed with the ScWpl1 N493E N622E (N419 and N547 in *A. gossypii*) mutations that our structure predicts would adversely interact with the conserved acidic residues at the C-terminal end of the WIS2 peptide. We next tested mutations in the conserved Wapl motifs 1 and 2, which lie at the N-terminal tip of the domain. Motif 1 forms an acidic patch, and includes the D272G mutation that has previously been identified as an *eco1-1* suppressor (Rowland *et al*, 2009), while motif 2 is the basic helix that projects from the side of the protein (Figure 2). We made conservative mutations that would be predicted to neutralise these charged patches, but not affect the folding of the protein. Both sets of mutations substantially reduced the binding of Wpl1 to Smc3, with a four-fold reduction in affinity seen with motif 2 mutations (Figure 6B; Table I). Inactivation or deletion of Wpl1 allows bypass of lethality associated with the *eco1-1* alleles. We tested the function of our binding mutants by introducing the proteins into an *eco1-1* strain from which *WPL1* had been deleted. The mutants were under the control of their endogenous promoter and were C-terminally HA tagged to allow detection. Western blot analysis verified that the mutant and wild-type proteins were expressed at the same level (Figures 6C and D). While re-introduction of wild-type Wpl1 totally blocks growth at the restrictive temperature, charge-neutralising mutations in motifs 1 and 2 rescue the cells, correlating with the reduction in Smc3 binding affinity observed *in vitro*, and demonstrating that the Wpl1–Smc3 interaction is physiologically relevant. Surprisingly, mutations in the WIS2 helix did not show strong rescue phenotypes (data not shown). This may reflect the fact that a simple weakening

 

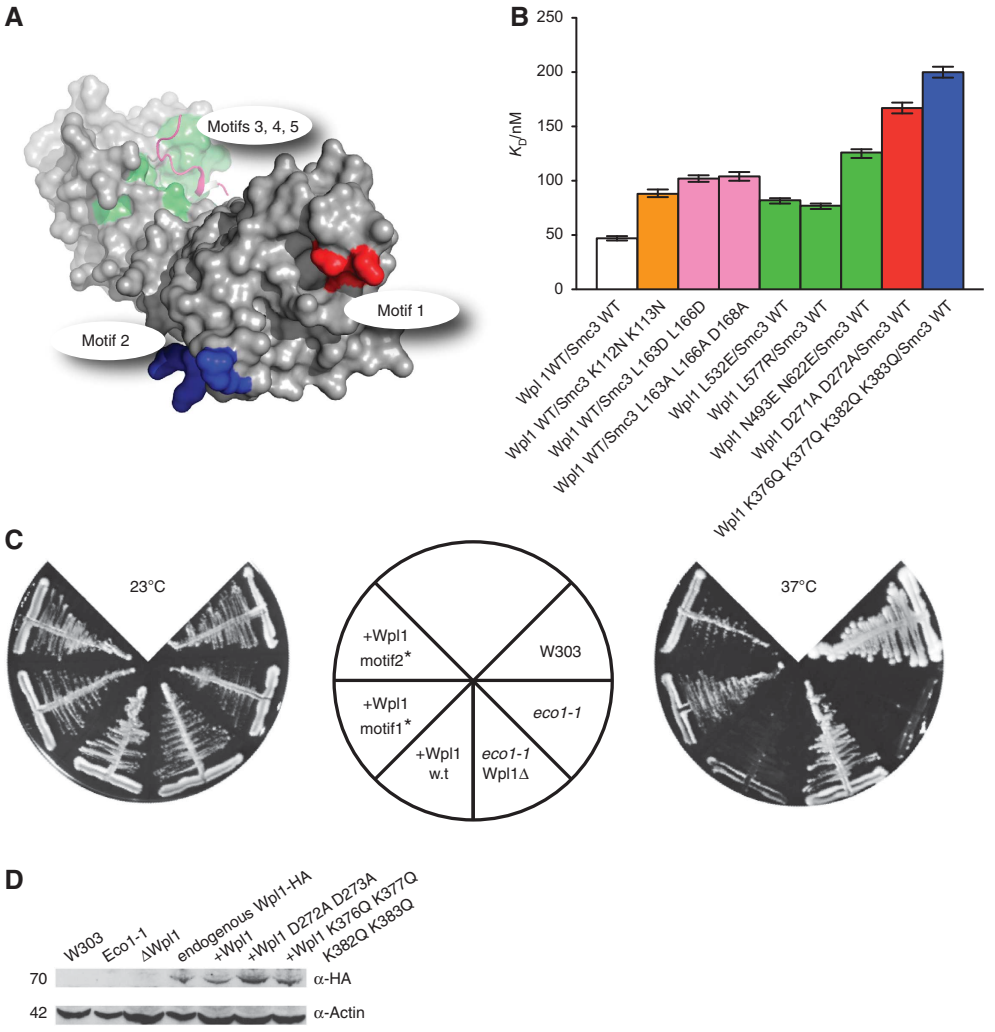


**Figure 6** Mutagenesis studies of the Wpl1–Smc3 interaction. (**A**) Diagram of the Wapl domain surface showing the location of the conserved motifs 1–5. (**B**) Binding constants of ScWpl1$^{259–647}$-ScSmc3AH mutants. The wild-type proteins are shown in white. Other mutants are coloured as follows: Smc3 WIS1—orange, Smc3 WIS2—pink, Wpl1 motifs 3,4,5—green, Wpl1 motif 1—red, Wpl1 motif 2—blue. Error bars are calculated from global fits of data obtained at eight different concentrations. (**C**) *In vivo* yeast viability assay of mutants in motifs 1 and 2. All mutants grow at the permissive temperature (left). At the restrictive temperature, mutants in motif 1 (D271A D272A) and motif 2 (K376Q K377Q K382Q K383Q) suppress lethality associated with loss of Eco1 function, indicating Wpl1 inactivation. (**D**) Cellular expression of the mutant proteins was verified by western blot. Expression levels of the mutant proteins were approximately similar to expression of wild-type Wpl1, both from the HA-tagged endogenous locus (lane 4) and introduced on an integrating plasmid (lane 5).

(as opposed to total disruption) of the interface is insufficient to affect the physiological function of the interaction, or that the molecular consequences of the mutations are not manifest by simple suppression of Eco1 deficiency.

## Discussion

In this study, we present the first structure of a member of the cohesin complex other than the core Smc1/Smc3/Scc1 subunits and show that it can directly bind the Smc3 ATPase via a conserved domain. Two of the three putative binding sites in Smc3 (WIS1 and WIS2) have been previously identified as being functionally important in either Smc3 or related ABC ATPases, and in this work, we show that mutations that are predicted to weaken binding to the third site involving the WIS3 demonstrate strong *in vivo* phenotypes. We discuss these points in more detail below. Further, we have shown that the strength of the interaction between Wpl1 and Smc3 is partially dependent on the acetylation state of the ATPase domain.

The Smc1–Smc3 heterodimer forms a functional ATPase, whose activity is necessary for correct loading of the cohesin complex onto chromosomes (Arumugam *et al*, 2003; Weitzer *et al*, 2003). The molecular details of ATP binding and hydrolysis by the ABC-ATPase superfamily have been extensively studied (Hopfner and Tainer, 2003), but how these processes relate to cohesion establishment is still unclear. Interestingly, the WIS2 site binding identified in this work has been previously proposed to be involved in ATP-driven conformational changes in other members of the ABC ATPase family, and there are precedents for protein–protein interactions involving regions structurally homologous to the WIS2. The sequence constitutes part of two short helices in Smc3 that link the nucleotide-interacting Q-loop (Hopfner *et al*, 2000) to the base of the coiled-coil domain (Figure 7A). These helices (termed as signature-coupling

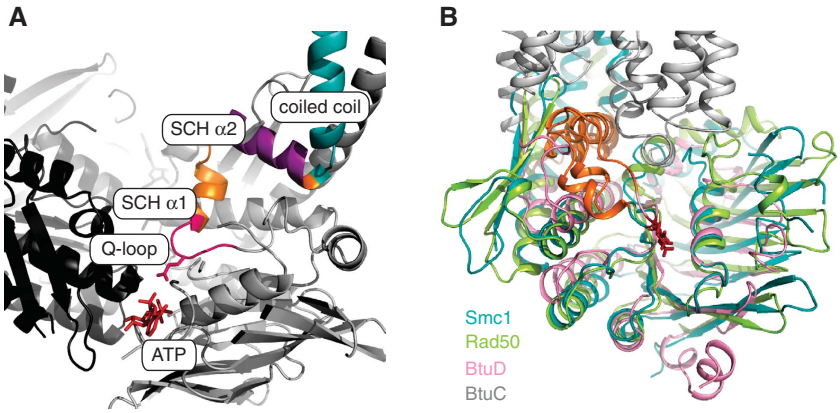


**Figure 7** Conservation and functional implications of the WIS2 helix. (**A**) Close up of the Smc1 ATPase active site, showing the location of the signature-coupling helices (purple and orange) between the Q-loop (pink) and the coiled coils (cyan). The predicted position of the WIS2 peptide bound to Wpl1 is depicted in purple. (**B**) Superimposition of ScSmc1 with the ATPase domain of Rad50 (pdb i.d. 3qkt) and BtuD (pdb i.d. 1l7v). The conserved glutamine that describes the Q-loop is shown in dark red, and the signature-coupling helices of Smc1 and Rad50 in orange. The transmembrane domain of the BtuC protein is shown in grey.

helices, SCH) have been previously described in the structurally homologous Rad50 ABC ATPase as being involved in the transduction of nucleotide-driven conformational changes (Williams *et al*, 2011). In Rad50, it has been proposed that nucleotide binding splays these helices apart, which in turn alters the orientation of the coiled coils relative to the ATPase domain. This might function to alter the association of other proteins with the ATPase domains. In other ABC ATPases involved in membrane transport processes, such as the BtuCD vitamin transporter (Locher *et al*, 2002) the transmembrane subunit binds the ATPase domain at a sequence directly adjacent to the Q-loop, so as to connect ATP-driven motion to conformational changes in a partner protein (Figure 7B). This raises the possibility that Wpl1 binding to Smc3 may modulate the ATPase activity of the cohesin complex, or transduce ATP-driven conformational transitions.

Assuming that Wpl1 binds the WIS2 in the same orientation in the full complex, the acidic C-terminal of the Wapl domain would sit close to the WIS1, while the amphoteric N-terminal domain, containing motifs 1 and 2 would project towards the coiled coils and WIS3. We expect that some conformational changes from the existing crystal structures of both Wpl1 and Smc3 might be required for full engagement of all three sites, and it is tempting to speculate that Wpl1 motif 2, located on the protruding basic helix in the N-terminal lobe of the protein, might undergo substantial repositioning upon binding to Smc3.

Our data show that the difference in affinity of Wpl1 for the acetylated and non-acetylated forms of Smc3 is relatively small, and likely arises from neutralisation of the positive charges on lysines K112 and K113. We predict therefore that the acetylation of cohesin may allow a structural change to occur in the ATPase domains, which may not require release of Wpl1 from the complex. This is consistent with results that show Wpl1 remains bound to cohesin throughout the cell cycle (Ben-Shahar *et al*, 2008). Equally, our mutations in the WIS2 and WIS3 reduced, but did not abolish binding of the Wapl domain to Smc3. This reflects the fact that multiple, large binding sites are relatively tolerant of a small number of mutations. Despite this, conservative point mutations that we predict would weaken the WIS3 interface are able to totally inhibit Wpl1 function. With current data, it is not entirely clear how these individual reductions in binding affinities cause these affects, but we propose that the mechanism involves Pds5, as this protein is required for destabilisation activity and can physically associate with Wpl1 (Rowland *et al*, 2009; Shintomi and Hirano, 2009; Sutani *et al*, 2009).

How the action of the 'anti-establishment' complex affects the stability of the cohesin–chromatin interaction is becoming clearer. A recent study has suggested that the predominant function of the Wpl1–Pds5 complex is to maintain an open Smc3–Scc1 interface to allow reversible association of cohesin with chromatin (Chan *et al*, 2012). In this model, the acetylation of Smc3 allows conformational changes to occur that cause a tightening of the cohesin–kleisin interaction and hence locks the complex onto chromatin. Previous structural studies (Haering *et al*, 2002) suggest that the relevant interface between Smc3 and the kleisin would be located near the base of the ATPase domains, which are adjacent to the WIS3 binding site. It will be important to establish, for example, if the interactions of Wpl1 with Smc3 and Scc1 are mutually exclusive.

Data from recent studies suggest that the cohesion establishment mechanism is highly complex and involves the regulated binding and conformational changes of a number of proteins in the cohesin complex. We propose that the conformation of the proteins, and interactions described in this study are relevant to a specific state in the establishment reaction, but other modes of binding might occur during the cohesin cycle together with associated conformational changes. Determining how these works will require further structural and biochemical studies to fully characterise the cohesin ATPase activity and dynamics of the protein associations within the complex.

## Materials and methods

### *Protein expression and purification*

The DNA sequences of the *A. gossypii* (residues 184–561) and *S. cerevisiae* (residues 259–647) orthologues of *WPL1* were cloned into a modified pET-28b(+) vector with a N-terminal His-tag sequence followed by a TEV protease cleavage site. The protein

 

was overexpressed in an *E. coli* BL21 (DE3) RIL expression strain. The cultures were grown until an $A_{600}$ of 0.6 units at 37°C and induced with 0.5 mM IPTG at 18°C for 16–18 h. Cells were lysed by sonication for 5 × 30 s and centrifuged at 34 000 *g* for 45 min in a buffer containing 50 mM Tris pH 7.5, 500 mM NaCl, 30 mM imidazole, 10 mM β-ME (buffer 1) supplemented with protease inhibitor tablets (Roche). The supernatant was incubated with Ni-Sepharose 6 Fast Flow beads (GE Healthcare) pre-washed in buffer 1 for 1 h at 4°C before washing with 10 column volumes of buffer 1. Elution was carried out using buffer 2 (50 mM Tris pH 7.5, 500 mM NaCl, 500 mM imidazole, 10 mM β-ME). The His tag was then cleaved by overnight incubation at 4°C with TEV protease at a ratio of 1:50 of protease to protein. Size exclusion chromatography using a Superdex 200 column (GE Healthcare) was then performed as a final purification step in the buffer 40 mM HEPES pH 7.5, 200 mM NaCl and 1 mM DTT. For selenomethionine (SeMet) labelling of AgWpl1$^{184–561}$, the recombinant plasmid was transformed into a B834+ strain of *E. coli* and grown in minimal LeMaster medium containing L-selenomethionine. The SeMet-labelled protein was purified as for the native protein.

The ScSmc3 head domain (residues1–190 and 1047–1231 with a linker consisting of residues SGGSGG) was expressed in a BL21(DE3) RIL strain, as a GST-fusion protein with a TEV cleavage site between the GST tag and protein sequence. Cultures were grown until an $A_{600}$ of 0.4 units at 37°C and induced with 0.5 mM IPTG at 18°C for 16–18 h. Cells were lysed in a buffer containing 50 mM Tris pH 8.0, 100 mM NaCl, 0.1% Tween-20, 1 mM DTT (buffer A) and centrifuged at 34 000 *g* for 45 min. The cleared lysate was incubated with glutathione Sepharose beads (GE Healthcare) pre-equilibrated in buffer A, for 2 h at 4°C. The beads were then washed with 10 column volumes of buffer B (50 mM Tris pH 8.0, 100 mM NaCl, 1 mM DTT) and the protein was finally eluted in the buffer C (50 mM Tris pH 8.0, 100 mM NaCl, 40 mM reduced glutathione, 1 mM DTT). Size exclusion chromatography was then carried out using a Superdex 200 column in a buffer containing 40 mM HEPES pH 8.0, 150 mM NaCl, 1 mM DTT.

### *Crystallisation, data collection and structure determination of AgWpl1$^{184–561}$*

Crystals were grown by hanging drop vapour diffusion at 4°C using protein at a concentration of 4 mg/ml. After optimisation, clusters of plate-like crystals were obtained in the buffer 0.1 M Na-K phosphate, 0.1 M bis-tris propane pH 7.5, 15% (w/v) PEG 3350. Single crystals were separated from the clusters and flash-frozen in the crystallisation buffer containing 20% (v/v) glycerol. Crystals of the SeMet-labelled protein could be grown in the same condition and had the same morphology as the native protein crystals. Diffraction data for both native and SeMet-labelled protein crystals were collected at the Diamond Light Source, UK. The data were processed and scaled using XDS (Kabsch, 2010) and SCALA (Evans, 2006). MAD phasing method using the AutoSHARP structure solution pipeline was used to solve the structure (Bricogne *et al*, 2003). An initial model was obtained using the program BUCCANEER (Cowtan, 2006) and further rounds of model building and refinement were carried out iteratively using COOT (Emsley *et al*, 2010) and REFMAC (Murshudov *et al*, 1997). All other operations were carried out using the CCP4 suite (Collaborative Computational Project, 1994). The structure was refined to a final R factor of 19.5% ($R_{free}$ = 22.9%) and validated using Coot and Molprobity tools (Lovell *et al*, 2003). The Ramachandran plot showed 96.9 and 0.42% of residues to be in the favoured and outlier regions, respectively. The structure figures were prepared using PyMol (www.pymol.org).

### *Crystallisation, data collection and structure determination of AgWpl1$^{184–561}$–WIS2 complex*

AgWpl1$^{184–561}$ and the WIS2 peptide were mixed in approximate molar ratios of 1:10 or 1:20 with a final protein concentration of 5 mg/ml. The protein–peptide mixture was incubated at 4°C on a rocking platform for 30 min before setting-up of the crystallisation screens. Crystals were grown at 4°C in a 96-well plate using sitting-drop vapour diffusion technique using a 400-nl drop size. The well solution used for growing the crystals contained 0.2 M ammonium sulphate, 0.1 M Tris pH 8.5 and 25% (w/v) PEG3350. The plate-like crystals were flash-frozen in the mother liquor supplemented with 30% (v/v) glycerol. Data were processed and scaled using XDS and SCALA. Molecular replacement using PHASER (McCoy *et al*, 2007) followed by a rigid-body refinement in REFMAC was used to trace and refine the peptide residues. To obtain a molecular replacement solution, the AgWpl1$^{184–561}$ protein was divided into domains 1, 2, and 3, and each domain used separately as a search model due to a conformational change in the liganded structure. The structure was refined to a final R factor of 24.6% ($R_{free}$ = 20.09%). The Ramachandran plot showed 96.8 and 1.36% of residues to be in the favoured and outlier regions, respectively.

### *Peptide arrays*

The ATPase head domain of Smc3 (residues 1–190 and 1045–1231), Smc1 (residues 1–190 and 1045–1222), and Scc1 (residues 1–597) from *A. gossypii* was arrayed on a cellulose membrane as peptide spots, each comprising 21 amino acids with a shift of 3 amino acids between successive peptides. The membrane was pre-incubated in a buffer containing 40 mM HEPES pH 7.5, 150 mM NaCl, 0.1% Tween-20, 0.25 mM TCEP (incubation buffer) and then 50 nM AgWpl1$^{184–561}$ added, and incubated overnight at 4°C. Blocking carried out in 40 mM HEPES pH 7.5, 150 mM NaCl, 0.1% Tween-20, 0.5% non-fat milk, 0.25 mM TCEP (blocking buffer) for 1 h at room temperature (RT). The array was then washed with incubation buffer for 3 × 10 min followed by probing with anti-AgWpl1$^{184–561}$ diluted 1:10 000 for 1 h at room temperature. The membrane was washed again with the incubation buffer for 3 × 10 min before adding the secondary antibody (goat anti-rabbit HRP conjugated, DAKO; 1:2000 dilution). As a control, the membrane was probed with antibodies in the absence of Wpl1 protein. The array was visualised using the ECL detection kit (GE Healthcare).

### *Fluorescence anisotropy peptide-binding assays*

Fluorescence anisotropy assays were carried out using fluorescein-labelled peptides and AgWpl1$^{184–561}$. The anisotropy was read using a Saffire$^2$ (Tecan) microplate reader in FP mode. The protein was dialysed into a buffer containing 20 mM Tris pH 7.5, 20 mM NaCl, 0.5 mM TCEP and the same buffer was used for dissolving and diluting peptides. The peptide concentration used was 50 nM while varying the protein concentration from 0 to 300 μM in a total volume 20 μl. The anisotropy readings were recorded after 1 h incubation at 4°C to allow attainment of equilibrium. Binding experiments were carried out in triplicate for each protein–peptide combination, and checked using multiple batches of protein. The formula used for the calculations was

$$Y = A_f + ((A_b - A_f) \times (X/(K_d + X)))$$

where $X$ is the protein concentration, $Y$ is the observed anisotropy, $A_b$ is anisotropy at saturation (anisotropy of the bound ligand), $A_f$ is anisotropy from the free ligand and $K_d$ is the equilibrium dissociation constant in same units as $X$. The data were analysed and the graphs were plotted using the software GraphPad (Prism).

### *Protein binding studies*

Binding studies between ScWpl1$^{259–647}$ and wild type and the GST-tagged ScSmc3 ATPase head (Smc3$^{AH}$) proteins were performed using an Octet RED (ForteBio). The Wpl1$^{259–647}$ was amine-coupled to the biosensor at a concentration of 12.5 μg/ml while the concentration of Smc3$^{AH}$ was varied (0, 25, 50, 100, 200, 400, 800, and 1200 nM). All the proteins for this assay were dialysed into the buffer 40 mM HEPES pH 7.5, 150 mM NaCl, 1 mM DTT. Control experiments using GST alone revealed no detectable interactions (Supplementary Figure 4e). Data were analysed and binding parameters calculated using the supplied software.

### *Yeast studies*

All yeast experiments were carried out in a W303 background. Strains are listed in Supplementary Table 2. Gene deletions and epitope tagging of the endogenous *WPL1* gene were carried out using standard PCR targeting techniques. Mutant versions of the *Wpl1* gene including 263 bases of upstream promoter region and sequences encoding a C-terminal 3 × HA epitope tag were cloned into a pYIpLac204 vector and introduced into the appropriate strain.

### *Thermal denaturation experiments*

Experiments were carried out with 5 μg of purified wild-type and mutant ScWpl1$^{259–647}$. The proteins were mixed with 5 μl of

50× SyPro Orange (Invitrogen) fluorescent dye and the final volume made up to 100 µl using a buffer containing 40 mM HEPES pH 7.5, 150 mM NaCl, and 1 mM DTT. The assay was performed in a 96-well plate using the iQ5 thermal cycler (Bio-Rad). The fluorescence signal was measured while ramping the temperature stepwise from 4 to 90°C with an increment of 0.5°C and a dwell time of 10 s at each step. The variation in the fluorescence signal has been interpreted as a graph of the differential of the fluorescence divided by the differential of temperature plotted against the temperature. The lowest point in each curve depicts the melting point or Tm of the respective protein.

#### *Structural data*

Atomic coordinates and structure factors have been deposited in the Protein Data Bank under accession codes 3zik ($AgWpl1^{184–561}$) and 3zil ($AgWpl1^{184–561}$–WIS2).

#### *Supplementary data*

Supplementary data are available at *The EMBO Journal* Online (http://www.embojournal.org).

## Acknowledgements

We wish to thank the LRI peptide synthesis unit and protein purification facility for reagents, H Walden for helpful discussions and F Uhlmann for extensive advice and provision of the *eco1-1* yeast strain. We also wish to thank V Borges, C Lehane, M Ocampo-Hafalla, A Purkiss-Trew, E Soriano and P Knowles for advice and assistance. X-ray data were collected on Diamond beamline IO4. This work was funded by Cancer Research UK.

*Author contributions*: AC cloned, purified, and crystallised the Wapl domain. All crystal structures were solved by AC and MRS. The Smc3 protein was cloned and purified by SZ. Peptide binding studies were carried out by AC. Protein binding studies were carried out by AC and SZ. Crystallisation of the protein–peptide complex was carried out by AC and X-WH. *In vivo* studies were carried out by MRS. The manuscript was written by MRS with input from other authors.

## Conflict of interest

The authors declare that they have no conflict of interest.

## References

Arumugam P, Gruber S, Tanaka K, Haering CH, Mechtler K, Nasmyth K (2003) ATP hydrolysis is required for cohesin's association with chromosomes. *Curr Biol* **13:** 1941–1953

Bellows AM, Kenna MA, Cassimeris L, Skibbens RV (2003) Human EFO1p exhibits acetyltransferase activity and is a unique combination of linker histone and Ctf7p/Eco1p chromatid cohesion establishment domains. *Nucleic Acids Res* **31:** 6334–6343

Ben-Shahar TR, Heeger S, Lehane C, East P, Flynn H, Skehel M, Uhlmann F (2008) Eco1-dependent cohesin acetylation during establishment of sister chromatid cohesion. *Science* **321:** 563–566

Borges V, Lehane C, Lopez-Serra L, Flynn H, Skehel M, Rolef Ben-Shahar T, Uhlmann F (2010) Hos1 deacetylates smc3 to close the cohesin acetylation cycle. *Mol Cell* **39:** 677–688

Bricogne G, Vonrhein C, Flensburg C, Schiltz M, Paciorek W (2003) Generation, representation and flow of phase information in structure determination: recent developments in and around SHARP 2.0. *Acta Crystallogr D Biol Crystallogr* **59:** 2023–2030

Chan K-L, Roig MB, Hu B, Beckouët F, Metson J, Nasmyth K (2012) Cohesin's DNA exit gate is distinct from its entrance gate and is regulated by acetylation. *Cell* **150:** 961–974

Collaborative Computational Project N (1994) The CCP4 suite: programs for protein crystallography. *Acta Crystallogr D Biol Crystallogr* **50:** 760–763

Cowtan K (2006) The Buccaneer software for automated model building. 1. Tracing protein chains. *Acta Crystallogr D Biol Crystallogr* **62:** 1002–1011

Emsley P, Lohkamp B, Scott WG, Cowtan K (2010) Features and development of Coot. *Acta Crystallogr D Biol Crystallogr* **66:** 486–501

Evans P (2006) Scaling and assessment of data quality. *Acta Crystallogr D Biol Crystallogr* **62:** 72–82

Game JC, Birrell GW, Brown JA, Shibata T, Baccari C, Chu AM, Williamson MS, Brown JM (2003) Use of a genome-wide approach to identify new genes that control resistance of Saccharomyces cerevisiae to ionizing radiation. *Radiat Res* **160:** 14–24

Gandhi R, Gillespie PJ, Hirano T (2006) Human Wapl is a cohesin-binding protein that promotes sister-chromatid resolution in mitotic prophase. *Curr Biol* **16:** 2406–2417

Groves MR, Hanlon N, Turowski P, Hemmings BA, Barford D (1999) The structure of the protein phosphatase 2A PR65/A subunit reveals the conformation of its 15 tandemly repeated HEAT motifs. *Cell* **96:** 99–110

Haering CH, Farcas A-M, Arumugam P, Metson J, Nasmyth K (2008) The cohesin ring concatenates sister DNA molecules. *Nature* **454:** 297–301

Haering CH, Löwe J, Hochwagen A, Nasmyth K (2002) Molecular architecture of SMC proteins and the yeast cohesin complex. *Mol Cell* **9:** 773–788

Haering CH, Schoffnegger D, Nishino T, Helmhart W, Nasmyth K, Löwe J (2004) Structure and stability of cohesin's Smc1-kleisin interaction. *Mol Cell* **15:** 951–964

Hirano T (2002) The ABCs of SMC proteins: two-armed ATPases for chromosome condensation, cohesion, and repair. *Genes Dev* **16:** 399–414

Holm L, Sander C (1993) Protein structure comparison by alignment of distance matrices. *J Mol Biol* **233:** 123–138

Hopfner K-P, Tainer JA (2003) Rad50/SMC proteins and ABC transporters: unifying concepts from high-resolution structures. *Curr Opin Struct Biol* **13:** 249–255

Hopfner KP, Karcher A, Shin DS, Craig L, Arthur LM, Carney JP, Tainer JA (2000) Structural biology of Rad50 ATPase: ATP-driven conformational control in DNA double-strand break repair and the ABC-ATPase superfamily. *Cell* **101:** 789–800

Ivanov D, Schleiffer A, Eisenhaber F, Mechtler K, Haering CH, Nasmyth K (2002) Eco1 is a novel acetyltransferase that can acetylate proteins involved in cohesion. *Curr Biol* **12:** 323–328

Kabsch W (2010) XDS. *Acta Crystallogr D Biol Crystallogr* **66:** 125–132

Kitajima TS, Kawashima SA, Watanabe Y (2004) The conserved kinetochore protein shugoshin protects centromeric cohesion during meiosis. *Nature* **427:** 510–517

Kueng S, Hegemann B, Peters BH, Lipp JJ, Schleiffer A, Mechtler K, Peters J-M (2006) Wapl controls the dynamic association of cohesin with chromatin. *Cell* **127:** 955–967

Lengronne A, McIntyre J, Katou Y, Kanoh Y, Hopfner K-P, Shirahige K, Uhlmann F (2006) Establishment of sister chromatid cohesion at the S. cerevisiae replication fork. *Mol Cell* **23:** 787–799

Locher KP, Lee AT, Rees DC (2002) The E. coli BtuCD structure: a framework for ABC transporter architecture and mechanism. *Science (New York, NY)* **296:** 1091–1098

Losada A, Hirano M, Hirano T (1998) Identification of Xenopus SMC protein complexes required for sister chromatid cohesion. *Genes Dev* **12:** 1986–1997

Lovell SC, Davis IW, Arendall WB, de Bakker PIW, Word JM, Prisant MG, Richardson JS, Richardson DC (2003) Structure validation by Calpha geometry: phi,psi and Cbeta deviation. *Proteins* **50:** 437–450

McCoy AJ, Grosse-Kunstleve RW, Adams PD, Winn MD, Storoni LC, Read RJ (2007) Phaser crystallographic software. *J Appl Crystallogr* **40:** 658–674

McGuinness BE, Hirota T, Kudo NR, Peters J-M, Nasmyth K (2005) Shugoshin prevents dissociation of cohesin from centromeres during mitosis in vertebrate cells. *PLoS Biol* **3:** e86

Murshudov GN, Vagin AA, Dodson EJ (1997) Refinement of macromolecular structures by the maximum-likelihood method. *Acta Crystallogr D Biol Crystallogr* **53:** 240–255

 

Nasmyth K (2001) Disseminating the genome: joining, resolving, and separating sister chromatids during mitosis and meiosis. *Annu Rev Genet* **35:** 673–745

Nishiyama T, Ladurner R, Schmitz J, Kreidl E, Schleiffer A, Bhaskara V, Bando M, Shirahige K, Hyman AA, Mechtler K, Peters J-M (2010) Sororin mediates sister chromatid cohesion by antagonizing Wapl. *Cell* **143:** 737–749

Rowland BD, Roig MB, Nishino T, Kurze A, Uluocak P, Mishra A, Beckouët F, Underwood P, Metson J, Imre R, Mechtler K, Katis VL, Nasmyth K (2009) Building sister chromatid cohesion: smc3 acetylation counteracts an antiestablishment activity. *Mol Cell* **33:** 763–774

Salic A, Waters JC, Mitchison TJ (2004) Vertebrate shugoshin links sister centromere cohesion and kinetochore microtubule stability in mitosis. *Cell* **118:** 567–578

Schleiffer A, Kaitna S, Maurer-Stroh S, Glotzer M, Nasmyth K, Eisenhaber F (2003) Kleisins: a superfamily of bacterial and eukaryotic SMC protein partners. *Mol Cell* **11:** 571–575

Schmitz J, Watrin E, Lénárt P, Mechtler K, Peters J-M (2007) Sororin is required for stable binding of cohesin to chromatin and for sister chromatid cohesion in interphase. *Curr Biol* **17:** 630–636

Shintomi K, Hirano T (2009) Releasing cohesin from chromosome arms in early mitosis: opposing actions of Wapl-Pds5 and Sgo1. *Genes Dev* **23:** 2224–2236

Skibbens RV (2009) Establishment of sister chromatid cohesion. *Curr Biol* **19:** R1126–R1132

Skibbens RV, Corson LB, Koshland D, Hieter P (1999) Ctf7p is essential for sister chromatid cohesion and links mitotic chromosome structure to the DNA replication machinery. *Genes Dev* **13:** 307–319

Sumara I, Vorlaufer E, Stukenberg PT, Kelm O, Redemann N, Nigg EA, Peters J-M (2002) The dissociation of cohesin from chromosomes in prophase is regulated by Polo-like kinase. *Mol Cell* **9:** 515–525

Sutani T, Kawaguchi T, Kanno R, Itoh T, Shirahige K (2009) Budding yeast Wpl1(Rad61)-Pds5 complex counteracts sister chromatid cohesion-establishing reaction. *Curr Biol* **19:** 492–497

Tanaka K, Hao Z, Kai M, Okayama H (2001) Establishment and maintenance of sister chromatid cohesion in fission yeast by a unique mechanism. *EMBO J* **20:** 5779–5790

Tang Z, Sun Y, Harley SE, Zou H, Yu H (2004) Human Bub1 protects centromeric sister-chromatid cohesion through Shugoshin during mitosis. *Proc Natl Acad Sci USA* **101:** 18012–18017

Tóth A, Ciosk R, Uhlmann F, Galova M, Schleiffer A, Nasmyth K (1999) Yeast cohesin complex requires a conserved protein, Eco1p(Ctf7), to establish cohesion between sister chromatids during DNA replication. *Genes Dev* **13:** 320–333

Uhlmann F, Wernic D, Poupart MA, Koonin EV, Nasmyth K (2000) Cleavage of cohesin by the CD clan protease separin triggers anaphase in yeast. *Cell* **103:** 375–386

Unal E, Heidinger-Pauli JM, Kim W, Guacci V, Onn I, Gygi SP, Koshland DE (2008) A molecular determinant for the establishment of sister chromatid cohesion. *Science* **321:** 566–569

Vernì F, Gandhi R, Goldberg ML, Gatti M (2000) Genetic and molecular analysis of wings apart-like (wapl), a gene controlling heterochromatin organization in Drosophila melanogaster. *Genetics* **154:** 1693–1710

Waizenegger IC, Hauf S, Meinke A, Peters JM (2000) Two distinct pathways remove mammalian cohesin from chromosome arms in prophase and from centromeres in anaphase. *Cell* **103:** 399–410

Warren CD, Eckley DM, Lee MS, Hanna JS, Hughes A, Peyser B, Jie C, Irizarry R, Spencer FA (2004) S-phase checkpoint genes safeguard high-fidelity sister chromatid cohesion. *Mol Biol Cell* **15:** 1724–1735

Weitzer S, Lehane C, Uhlmann F (2003) A model for ATP hydrolysis-dependent binding of cohesin to DNA. *Curr Biol* **13:** 1930–1940

Williams GJ, Williams RS, Williams JS, Moncalian G, Arvai AS, Limbo O, Guenther G, Sildas S, Hammel M, Russell P, Tainer JA (2011) ABC ATPase signature helices in Rad50 link nucleotide state to Mre11 interface for DNA repair. *Nat Struct Mol Biol* **18:** 423–431

Zhang J, Shi X, Li Y, Kim B-J, Jia J, Huang Z, Yang T, Fu X, Jung SY, Wang Y, Zhang P, Kim S-T, Pan X, Qin J (2008) Acetylation of Smc3 by Eco1 is required for S phase sister chromatid cohesion in both human and yeast. *Mol Cell* **31:** 143–151